Structure and Bonding 131

Molecular Thermodynamics of Complex Systems

Bearbeitet von
Xiaohua Lu, Ying Hu

1. Auflage 2008. Buch. ix, 274 S. Hardcover
ISBN 978 3 540 69114 3
Format (B x L): 15,5 x 23,5 cm

Struct Bond
DOI:10.1007/430_2008_2

Thermodynamic Modeling of Complex Systems

Matthias Kleiner, Feelly Tumakaka, and Gabriele Sadowski

Abstract The thermodynamic behavior of complex pure fluids and mixtures is strongly affected by specific interactions like association (hydrogen bonding) and electrostatic interactions of permanent or induced dipoles. The modeling of those systems requires a physical model that is able to explicitly account for these specific interactions. This contribution describes the state of the art in modeling of complex fluids using analytical equations of state. Many applications demonstrate that those models can successfully be applied to describe and even to predict the phase behavior of a whole variety of substances ranging from small gas molecules up to organic solvents and polymeric systems.

Keywords: Copolymers · Pharmaceutical · Phase equilibria · Polymers

Contents

M. Kleiner, F. Tumakaka, and G. Sadowski(✉)
Dortmund University of Technology, Laboratory of Thermodynamics,
Emil-Figge-Str. 70, 44227 Dortmund, Germany
e-mail: gabriele.sadowski@bci.tu-dortmund.de

1 Introduction

The ability to predict and to correlate thermodynamic properties and phase equilibria is essential for the simulation of chemical processes and thus for process development and optimization. For industrial as well as for academic applications, the applied models should possess a sufficient accuracy over a wide range of conditions using a minimum of adjustable and easily accessible parameters.

Significant progress towards this type of model was made by applying the approach of perturbation theories from statistical mechanics. These theories are based on the fact that the thermodynamic properties of a system are mainly determined by the repulsive interactions of the molecules. Thus, these theories typically choose a reference system that shows only repulsive interactions. An often used reference systems is a system of "hard spheres," which have a fixed volume and no other interactions than repulsion. Starting from that, the influence of any deviation of a real system from the reference system to the thermodynamic behavior is described as a perturbation of the repulsive reference system. These deviations might be van der Waals attractive interactions, specific interactions like association, polar or quadrupolar interactions as well as the non-spherical shape of the molecules. Usually, these perturbations are assumed to be additive and independent of each other.

A whole series of models of this kind is based on the statistical associating fluid theory (SAFT) [1–4], which considers a molecule as a chain of tangent spherical segments. Starting from the Helmholtz energy of a hard-sphere reference system A^{hs}, different perturbation contributions are considered. These are namely the hard-sphere chain formation of m segments (A^{chain}), which accounts for the non-spherical shape of molecules, non-specific attractive interactions (A^{disp}) of the m (non-bonded) spherical segments, and very strong, short-range attractive interactions, like association (A^{assoc}).

Thus, the total Helmholtz energy of a system can be written as:

$$A^{\mathrm{res}} = mA^{\mathrm{hs}} + mA^{\mathrm{disp}} + A^{\mathrm{chain}} + A^{\mathrm{assoc}}. \tag{1}$$

Within the SAFT model, the Helmholtz energy of the reference A^{hs} is described using the Carnahan–Starling expression [5]; the segment–segment dispersion contribution to the Helmholtz energy A^{disp} is described using a fourth-order perturbation term [6, 7]. The contribution of chain formation as well as the association term are accounted for, based on the work of Wertheim [8].

Subsequently, several models were suggested that differ in the use of the various perturbation expressions. Examples are the perturbed hard-sphere-chain theory (PHSC) [9], as well as the models proposed by Chang and Sandler [10], Gil-Villegas et al. [11], and Hino and Prausnitz [12].

Each of these models considers the non-spherical shape of a molecule on one-hand side and the attractive interaction on the-other-hand side as independent perturbations of the reference system. Several attempts have been made to overcome this deficiency. Various models were suggested that use attractive square-well spheres

(e.g., [11, 13, 14]) or Lennard-Jones spheres (e.g., [15–17]) rather than hard spheres as reference to modify the chain contribution A^{chain}.

The perturbed-chain SAFT (PC-SAFT) model [18, 19] adopts the opposite idea: here, a perturbation theory of second order is applied to the reference system of hard chains instead of hard spheres to develop a dispersion term A^{disp}. Whereas the contributions to describe the hard-chain formation as well as the association are identical to those of the original SAFT model, the dispersion term was modified to account for the influence of the non-spherical shape of the molecule on the number of intermolecular interactions, and is therefore a function of segment number m:

$$A^{\text{res}} = A^{\text{hc}} + A^{\text{disp}}(m) + A^{\text{assoc}}. \tag{2}$$

The PC-SAFT model was successfully applied to a wide variety of systems, demonstrating that the modeling results could be improved for more systems than just for chain molecules like polymers. Even for small non-spherical substances, the modeling results could be improved considerably compared to the original SAFT model [18–21].

In addition to dispersive interactions, the phase behavior of pure fluids and mixtures is strongly affected by specific intermolecular interactions like association (hydrogen bonding) or dipolar interactions. Müller and Gubbins [22] gave a detailed review of different approaches to describe the contribution of association interactions to the Helmholtz energy A^{assoc} of a system, and discussed numerous examples of its application to real fluids and mixtures.

To account for dipolar interactions, various theories based on statistical mechanics were developed. In these theories, the dipole moment is assumed to be positioned at the center of a sphere, whereas the diameter of the sphere is chosen to preserve the molecular volume [23–31]. This treatment, however, does not explicitly account for the non-spherical shape, which becomes important in many real dipolar fluids, and thus its application is limited to simple fluids and mixtures. To account for the non-spherical shape of dipolar molecules, Jog and Chapman [32] proposed a theory that considers polar molecules as chains of non-polar and dipolar spherical segments. Another way to account for the non-spherical shape of dipolar molecules was followed by Gross and Vrabec [33], who assumed a two-center Lennard–Jones fluid as reference fluid. The model constants were adjusted to simulation data of two-center Lennard–Jones molecules having different molecular elongations from spheres up to dimers. The model was applied with PC-SAFT and is referred to as perturbed-chain polar SAFT (PCP-SAFT).

An alternative route to the perturbation theories was followed by Saager and Fischer [34] and Saager et al. [35] who constructed a dipolar contribution to the Helmholtz free energy on the basis of computer simulation results by fitting empirical expressions to simulation data of two-center Lennard–Jones molecules.

However, all these dipole expressions do not account for the polarizability of molecules that allows the induction of a dipolar moment in a molecule. To account for the non-additive induction interactions due to the polarization of molecules, Kleiner and Gross [36] applied the renormalized perturbation theory of Wertheim

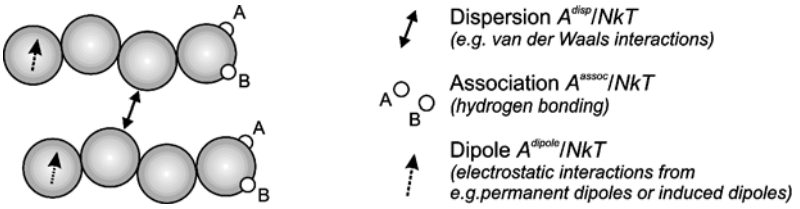

Fig. 1 Molecular picture of the PC-SAFT equation of state and its extension to dipolar fluids (e.g., PCP-SAFT, PCIP-SAFT). Illustration of the perturbation contributions to account for dispersion interactions, association interactions, and dipolar interactions

[37, 38] in combination with the dipolar expression of Gross and Vrabec. The equation of state contribution was applied with PC-SAFT to real fluids and mixtures and the model is referred to as perturbed-chain induced-polar SAFT (PCIP-SAFT).

The underlying molecular picture of the PC-SAFT equation of state, as well as of its extensions to dipolar and polarizable fluids (e.g., PCP-SAFT, PCIP-SAFT), is depicted in Fig. 1.

Thus, the Helmholtz energy using PC-SAFT based models finally reads as:

$$A^{\mathrm{res}} = A^{\mathrm{hc}} + A^{\mathrm{disp}}(m) + A^{\mathrm{assoc}} + A^{\mathrm{dipole}}. \tag{3}$$

Many applications of PC-SAFT as well as of its extensions for polar and polarizable fluids (PCP-SAFT and PCIP-SAFT) demonstrated that these models can successfully be applied to a broad range of substances and mixtures including simple fluids without specific interactions, associating fluids as well as to dipolar components and their mixtures. The model was applied to aqueous electrolyte solutions [39] as well as to solutions of aqueous amino acids and polypeptides [40]. An excellent performance of the PC-SAFT model was also shown for various polymer as well as copolymer systems.

This contribution summarizes the state of the art in modeling using PC-SAFT-based models. Due to the wide variety of compounds and the resulting mixtures, the focus lies on the modeling of phase equilibria of very asymmetric mixtures that exhibit complex intermolecular interactions.

2 PC-SAFT Equation of State

According to Eq. 3, different contributions to the Helmholtz energy are considered in PC-SAFT. They are briefly described below. The detailed expressions for each contribution can be found in the appendix.

2.1 Hard-Chain Contribution A^{hc}

The hard-chain reference fluid consists of spherical segments that do not show any attractive interactions. It is defined by two parameters, namely the number of segments m and the diameter of segments σ. The Helmholtz energy of this reference system is described by an expression developed by Chapman et al. [41], which is based on Wertheim's first-order thermodynamic perturbation theory [42–44].

2.2 Dispersion Contribution A^{disp}

To determine the contribution of dispersive attractions to the Helmholtz energy of a system, PC-SAFT applies the perturbation theory of Barker and Henderson [45, 46] to the hard-chain reference system instead of the hard-sphere system. Thus, the influence of the non-spherical shape of molecules on the attractive dispersion interactions is explicitly considered.

In addition to the above-mentioned parameters, segment number m and segment diameter σ, one additional parameter is required for describing the segment–segment interaction: the dispersion energy parameter ε/k. All three parameters are determined by simultaneously fitting to liquid density and vapor-pressure data of a pure component. The parameter-estimation approach for non-volatile substances, such as solids or polymers, is later described in the solid–liquid equilibria (Sect. 4) and polymer (Sect. 5) sections, respectively.

To model mixtures, conventional Berthelot–Lorentz combining rules are applied:

$$\sigma_{ij} = \frac{1}{2}(\sigma_i + \sigma_j), \tag{4}$$

$$\varepsilon_{ij} = \sqrt{\varepsilon_i \varepsilon_j} \cdot (1 - k_{ij}). \tag{5}$$

Equation 5 contains one adjustable binary interaction parameter k_{ij}, which is used to correct the dispersion energy in the mixture. If needed, this is determined from fitting to phase-equilibrium data of the binary mixture. Parameter k_{ij} will remain the only parameter that is fitted to binary data and is usually independent of temperature. For the description of ternary of higher systems it is assumed that the system is dominated by two-molecule interactions and thus no parameters other than the binary parameters are required.

2.3 Association Contribution A^{assoc}

The contribution due to short-range association interactions (hydrogen bonding) A^{assoc} is considered by an association model that was proposed by Chapman et al.

[2,41] based on Wertheim's first-order thermodynamic perturbation theory (TPT1). Within this theory, a molecule is assumed to have one or more association sites that can form hydrogen bonds. This is shown exemplarily in Fig. 1 for molecules with two association sites A and B. The association between two association sites is characterized by two additional parameters: the association energy $\varepsilon^{A_iB_i}/k$ and the effective volume of an association interaction $\kappa^{A_iB_i}$. Therefore, an associating compound is characterized by five pure-component parameters.

The number of association sites of a molecule and the possible site–site interactions have a profound effect on the fluid structure, and therefore on the phase behavior, and should thus be chosen carefully. Examples are given later in this contribution (see Sect. 3.3).

The strength of cross-association interactions between two different associating compounds can be determined using simple combining rules of the pure-component parameters, as suggested by Wolbach and Sandler [47] without introducing binary parameters:

$$\varepsilon^{A_iB_j} = \frac{1}{2}\left(\varepsilon^{A_iB_i} + \varepsilon^{A_jB_j}\right), \tag{6}$$

$$\kappa^{A_iB_j} = \sqrt{\kappa^{A_iB_i}\kappa^{A_jB_j}}\left(\frac{\sqrt{\sigma_{ii}\sigma_{jj}}}{1/2\,(\sigma_{ii}+\sigma_{jj})}\right)^3. \tag{7}$$

2.4 Dipole/Polarizability Contribution A^{dipole}

Long-range electrostatic interactions of dipolar and polarizable fluids A^{dipole} are taken into account by the expression of Kleiner and Gross (PCIP-SAFT). It is based on the renormalized perturbation theory for polarizable polar fluids of Wertheim [37,38], which was applied to the dipole contribution for non-spherical molecules of Gross and Vrabec. Since tabulated values for the dipole moments and average molecular polarizabilities are available, no additional adjustable parameters are required.

For non-polarizable components, the dipolar expression of Gross and Vrabec is recovered and, thus, the PCIP-SAFT equation of state simply reduces to PCP-SAFT.

3 Modeling of Low Molecular Weight Systems

The PC-SAFT equation of state can successfully be applied to correlate or even to predict the thermodynamic properties of a broad range of low molecular weight substances (e.g., [18, 20]). For systems without specific interactions (e.g., alkane mixtures) the phase behavior as well as the heat of mixing can usually even be predicted ($k_{ij} = 0$) in good agreement with experimental data. This is illustrated in Fig. 2 for the mixture of hexane and hexadecane.

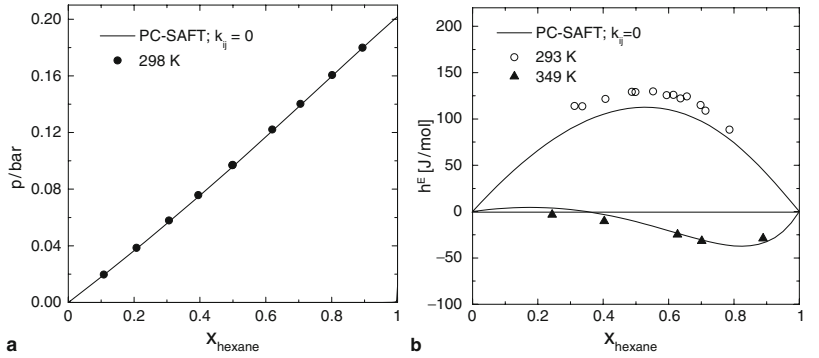

Fig. 2 PC-SAFT predictions ($k_{ij} = 0$) (*lines*) of thermodynamic properties of the mixture hexane/hexadecane at different temperatures in comparison to experimental data (*symbols*). **a** Vapor–liquid equilibrium at $T = 298\,\mathrm{K}$ (*filled circles* experimental data from Shen et al. [48]). **b** Excess enthalpies at two temperatures (*open circles* experimental data from McGlashan and Morcom [49], *filled triangles* experimental data from Holleman [50])

However, modeling of strongly asymmetric mixtures and mixtures exhibiting complex intermolecular interactions is much more challenging and will be discussed in the following section.

3.1 Mixtures of Strongly Polar and Non-polar Fluids

Mixtures containing polar as well as non-polar components often exhibit a strong deviation from ideality, and thus often show an azeotropic behavior. It was shown in several investigations that these mixtures can only be described accurately when the specific electrostatic interactions are explicitly taken into account.

The PCIP-SAFT model is applied here to model the thermodynamic behavior of strongly dipolar fluids and their mixtures with non-polar compounds, both of which are polarizable. An example of such a mixture is the binary system *N*,*N*-dimethylformamide and 1-butene, which is shown in Fig. 3. In order to assess the effect of the polarizability, the results are compared to the PCP-SAFT model where only permanent dipoles are considered. Moreover, the results are compared to the original PC-SAFT model where the electrostatic interactions are not explicitly accounted for. It becomes obvious that both PCIP-SAFT and PCP-SAFT are in good agreement with the experimental data, while the non-polar PC-SAFT model reveals a false temperature-behavior in describing a non-physical liquid–liquid demixing at lower temperatures.

Moreover, the physically more realistic models PCIP-SAFT and PCP-SAFT require a much lower value of the binary parameter than the non-polar PC-SAFT, while providing a superior description of the experimental data.

Another example for the strong influence of dipolar interactions on the thermodynamic properties is the mixture butyronitrile and *n*-heptane. The vapor–liquid equilibrium of this mixture at $T = 318\,\mathrm{K}$ is depicted in Fig. 4a. When a binary interaction

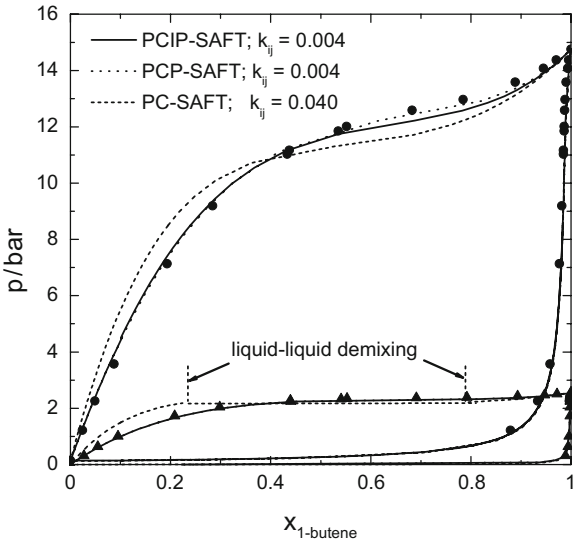

Fig. 3 Vapor–liquid equilibrium of the mixture *N*,*N*-dimethylformamide/1-butene at two temperatures (*filled circles* 363 K, *filled triangles* 293 K). Comparison of experimental data from Wilding et al. [51]to correlation results of PCIP-SAFT, of PCP-SAFT, and of PC-SAFT

parameter of the non-polar PC-SAFT model is adjusted, the model is not capable of reproducing the vapor–liquid equilibrium. Taking into account the polarity of butyronitril as well as the polarizibility of the two components, the PCIP-SAFT model provides a good representation of the experimental data, while the binary interaction parameter is almost zero. Although the binary interaction parameter is somewhat higher for the PCP-SAFT model, it is in almost as good agreement with the data. This is substantiated in Fig. 4b, where the predicted excess enthalpies of PCIP-SAFT and PCP-SAFT are in qualitative good agreement with the experimental data, compared to the non-polar PC-SAFT model.

It can be concluded that when considering this type of mixture, the inclusion of dipolar interaction and induced dipolar interactions due to the molecule's polarizability usually leads to lower (absolute) values of the required binary interaction parameter. Thus, the predictive abilities of the model are significantly improved when the physics of the molecules is considered. In particular, the consideration of the dipole moments in PCP-SAFT leads to a remarkable improvement of the modeling results compared to the non-polar PC-SAFT model. An additional accounting for the molecular polarizabilities in PCIP-SAFT usually leads to a further improvement of the modeling compared to PCP-SAFT.

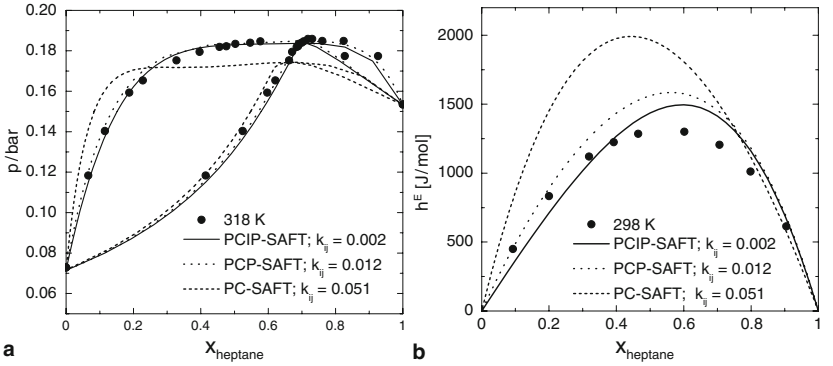

Fig. 4 Thermodynamic properties of the mixture butyronitrile/*n*-heptane. **a** Vapor–liquid equilibrium at $T = 318\,\mathrm{K}$. Comparison of experimental data from Artal et al. [52] (*filled circles*) to correlation results of PCIP-SAFT, of PCP-SAFT, and of PC-SAFT. **b** Excess enthalpies of mixing at 298 K. Predictions of PCIP-SAFT, of PCP-SAFT, and of PC-SAFT and comparison to experimental data from Akamatsu et al. [53] (*filled circles*). Binary interaction parameters were adjusted to VLE data as shown in **a**

3.2 Mixtures of Polar and Associating Fluids

The modeling of mixtures containing polar as well as associating components is very challenging for any equation of state. This is due to the fact that classical combining rules do not allow for the consideration of cross-interactions of molecules showing unlike interactions as pure components. Here, mixtures of a self-associating component (e.g., water) in a mixture with a component that does not self-associate but can act as either proton donor (e.g., chloroform) or proton acceptor (e.g., acetone) are considered. In those mixtures, cross-association interactions may occur: the polar compound does not self-associate but is able to associate with the associating compound. This type of interaction is here referred to as induced association to distinguish from mixtures of two self-associating compounds for which the combining rules (Eqs. 6 and 7) can directly be applied. However, using a simple but physical meaningful approach it is possible to account for the induced cross-association only from the knowledge of the pure-component parameters [54].

This approach is based on the following assumptions:

1. The association-energy parameter $\varepsilon^{\mathrm{A}_i\mathrm{B}_i}$ of the non-self-associating (polar) component is set to zero
2. The association-volume parameter $\kappa^{\mathrm{A}_i\mathrm{B}_i}$ of the non-self-associating component is assumed to be equal to the value of the associating component in the mixture

As a consequence of the first assumption, association of the polar substance is considered only if the mixture contains at least one associating component. Based on these assumptions, the cross-association parameters in the mixture can simply be calculated by applying the combining rules of Wolbach and Sandler (Eqs. 6 and 7).

The advantage of this approach is that the cross-association parameters are easily accessible and that no additional adjustable parameters are required.

Some applications of the proposed approach to model vapor–liquid as well as liquid–liquid equilibria of mixtures will be presented. Any effects due to polarizability are not explicitly considered here since they were found to have a minor influence on the phase behavior in these mixtures and, thus, the PCP-SAFT model is used for the polar compounds. All results are compared with calculations using PCP-SAFT and the classical approach where induced-association interactions are not considered.

Figure 5 shows the error bars of predicted ($k_{ij} = 0$) bubble-point pressures for different mixtures of alcohols with polar compounds. The grey bars show predictions using the classical approach where the induced-association interactions are not considered. The black bars represent predictions where the induced association between the associating and the polar component is explicitly accounted for. It can be seen that the deviations of the experimental and calculated bubble-point pressures can be drastically reduced especially for the mixtures containing methanol or ethanol. Since the influence of the OH-groups decreases with increasing chain length of the alcohols, the influence of the induced association also decreases. Nevertheless, the bubble-point predictions can still be improved for longer alcohols when the proposed approach for induced association is applied.

The phase behavior of a mixture of water and methyl methacrylate at atmospheric pressure is depicted in Fig. 6. This system shows heteroazeotropic behavior with a vapor–liquid equilibrium at higher temperatures and a liquid–liquid demixing at lower temperatures. Using the classical approach, the heteroazeotropic behavior in this mixture cannot be described quantitatively even using a very high binary interaction parameter. When the induced association is considered, the phase equilibrium can even be predicted setting the binary interaction parameter to zero.

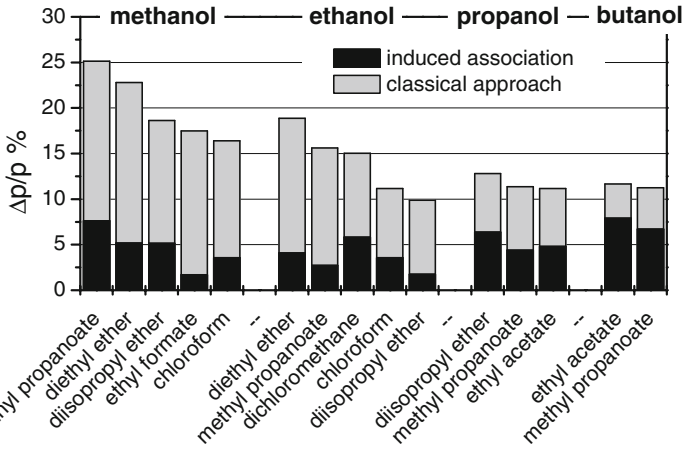

Fig. 5 Error bars of predicted bubble-point pressures for different alcohols in mixtures with a second component, which is polar

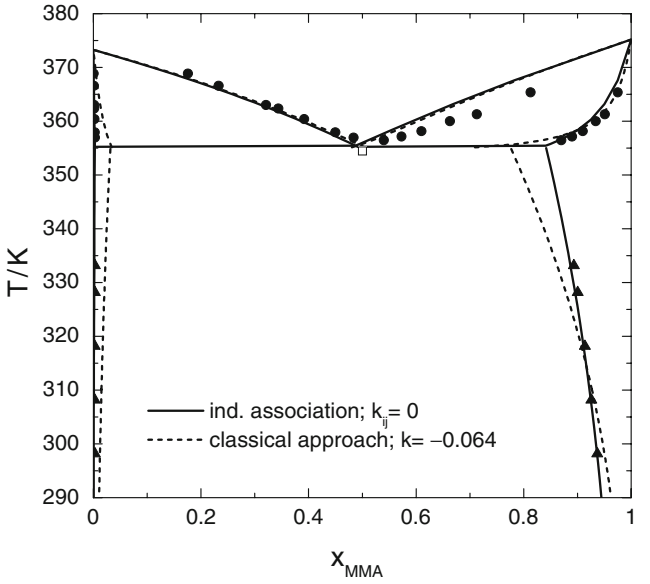

Fig. 6 Liquid–liquid and vapor–liquid equilibrium of the mixture methyl methacrylate (MMA)/water at $p = 1$ bar (*filled circles* Danov et al. [55], *open square* Frolova et al. [56], *filled triangles* Fu et al. [57]). *Dashed lines*: correlation results of PCP-SAFT using the classical approach. *Solid lines*: PCP-SAFT predictions considering the induced association

The approach can also be extended to ternary mixtures. Figure 7 shows the liquid–liquid equilibrium of the ternary mixture water/furfural/ethyl acetate as an example of a mixture with one associating component that may form cross-associates with the two polar compounds furfural and ethyl acetate. The binary interaction parameters for water/furfural and water/ethyl acetate are taken from the binary subsystems and the k_{ij} for the system ethyl acetate/furfural is set to zero. Thus, the ternary liquid–liquid equilibrium is predicted using only the binary information of the subsystems water/furfural and water/ethyl acetate, respectively. It becomes obvious that again the predicted results are in very good agreement with experimental data when the induced association is considered, whereas the classical approach is not able to properly describe the ternary-mixture phase behavior.

This is substantiated in Fig. 8 for the system water/methanol/methyl methacrylate. The classical approach underestimates the miscibility gap, even if a binary interaction parameter is used for the water/methyl methacrylate binary system, whereas the liquid–liquid equilibrium can be well predicted when applying the approach for the induced association.

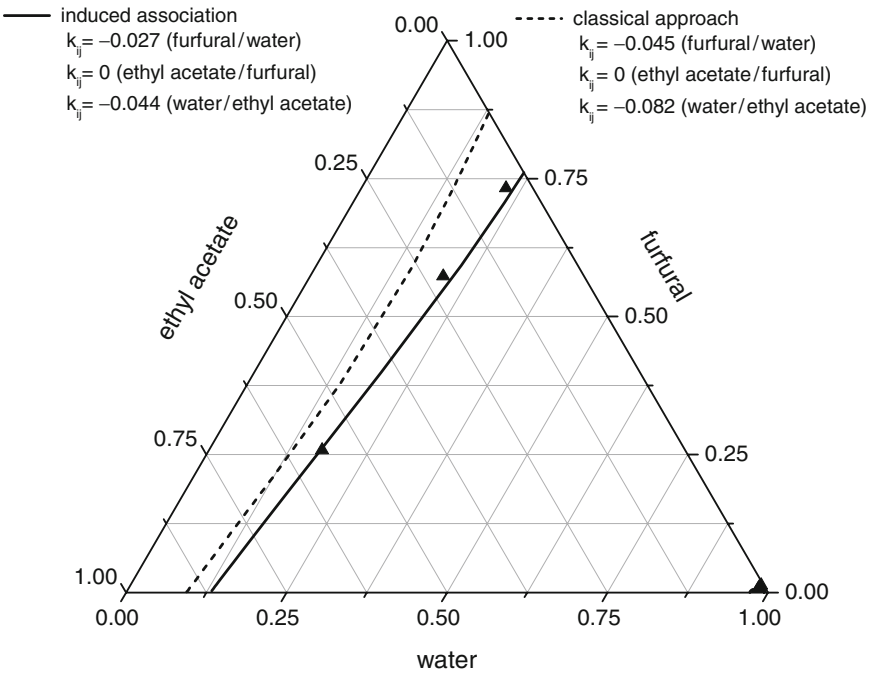

Fig. 7 Liquid–liquid equilibrium of the ternary mixture water/furfural/ethyl acetate for $T = 298\,\mathrm{K}$ (*filled triangles* Lloyd et al. [58]). *Dashed line*: predictions of PCP-SAFT using the classical approach. *Solid line*: PCP-SAFT predictions considering the induced association

3.3 Mixtures with Carboxylic Acids

In general, carboxylic acids are well described using two different association sites: a donor site at the oxygen and an acceptor site at the OH-group [20,61]. This corresponds to the 2B-association scheme as suggested by Huang and Radosz [3].

However, particularly small carboxylic acids show a specific thermodynamic behavior (e.g., very high boiling points), which is caused by two hydrogen bonds formed between the carboxylic groups of two acid molecules (see Fig. 9).

Therefore, these acid molecules appear as cyclic dimers even in the vapor phase.

This behavior can be captured using PC-SAFT by allowing for only one association site per molecule (1A-association scheme). A schematic picture of the 1A- and 2B-association schemes and the possible site–site interactions of the association sites are depicted in Fig. 10. As can be seen from Fig. 10a, the 1A-association enables the formation of only dimers whereas the 2B-scheme would also allow the formation of clusters with more than two molecules.

Investigations of pure-component properties of different carboxylic acids (from formic acid up to decanoic acid) showed that using a one-site association scheme gives an improved representation of liquid-density data and in particular of vapor-pressure data. For example, the unweighted average of all individual AAD values

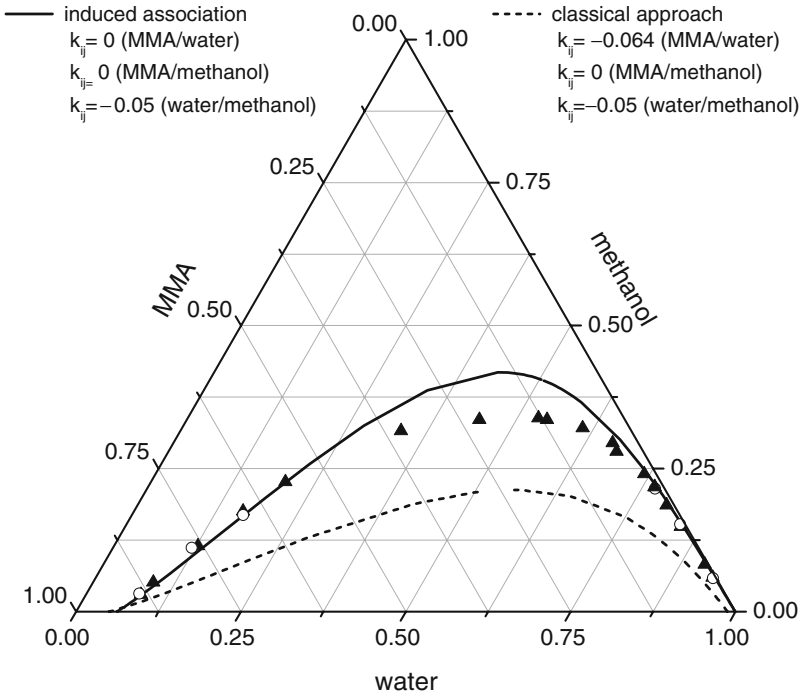

Fig. 8 Liquid–liquid equilibrium of the ternary mixture water/methanol/methyl methacrylate (MMA) for $T = 298\,\mathrm{K}$ (*open circles* Clausse et al. [59], *filled triangles,* Chubarov et al. [60]). *Dashed line*: predictions of PCP-SAFT using the classical approach. *Solid line*: PCP-SAFT predictions considering the induced association

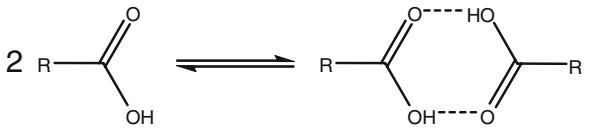

Fig. 9 Dimerization of carboxylic acids

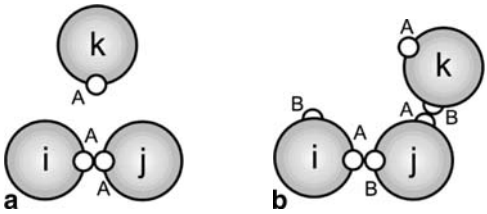

Fig. 10 Site–site interactions assumed by two different association schemes as suggested by Huang and Radosz [3]

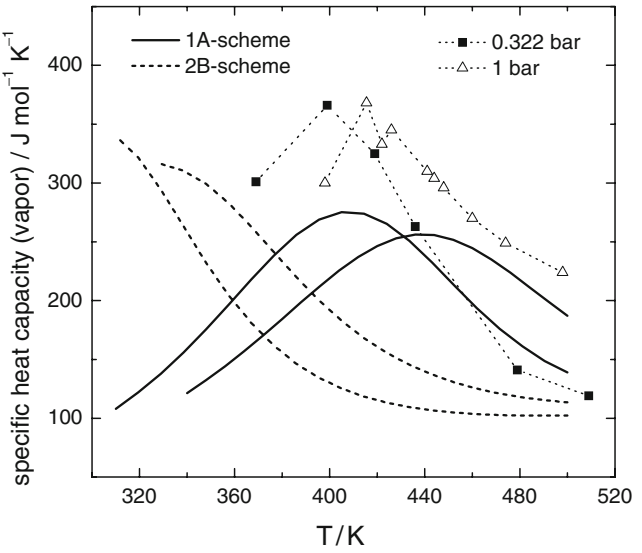

Fig. 11 Specific heat capacities (vapor phase) for acetic acid at two pressures (*filled squares* for $p = 0.332$ bar, *open triangles* for $p = 1$ bar). *Dashed lines*: Predictions via PC-SAFT using the 2B-association scheme. *Solid lines*: PC-SAFT predictions using the 1A-association scheme. Experimental data are taken from Weltner [62]

for vapor pressure data are 1.08% for the 1A scheme and 3.24% for the 2B scheme. For the liquid densities, average errors of 0.93% and of 1.28% were obtained for the 1A- and 2B-association schemes, respectively.

The specific heat capacities of acetic acid in the vapor phase are depicted in Fig. 11 at 0.33 bar and 1 bar, respectively. The experimental data show a maximum of the heat capacity. As can be seen, the predictions using the 1A scheme also follow this behavior and are in qualitative agreement to the experimental data, whereas the results obtained with the 2B scheme do not show this trend in the respective temperature range. This is quite remarkable because the heat capacities were not used for the determination of the acid pure-component parameters. These results reveal the good performance of the 1A scheme for the modeling and even prediction of pure-component properties of carboxylic acids.

The 1A- and 2B-association schemes are also compared for modeling the phase behavior of binary mixtures with acetic acid. The mixture of acetic acid with the non-polar cyclohexane as depicted in Fig. 12 is an example of a mixture in which the acid does not cross-associate but is only able to form self-associates. The dashed line indicates correlations using the 2B-association scheme where dimerization is not accounted for. It can be seen that the correlations are in poor agreement with the experimental data. If the dimerization is considered by applying the 1A-association scheme, the quality of the correlations can be improved considerably.

Considering the system acetic acid/carbon dioxide (Fig. 13), the carbon dioxide molecule may form weak hydrogen bonds with the carboxyl group of acetic acid.

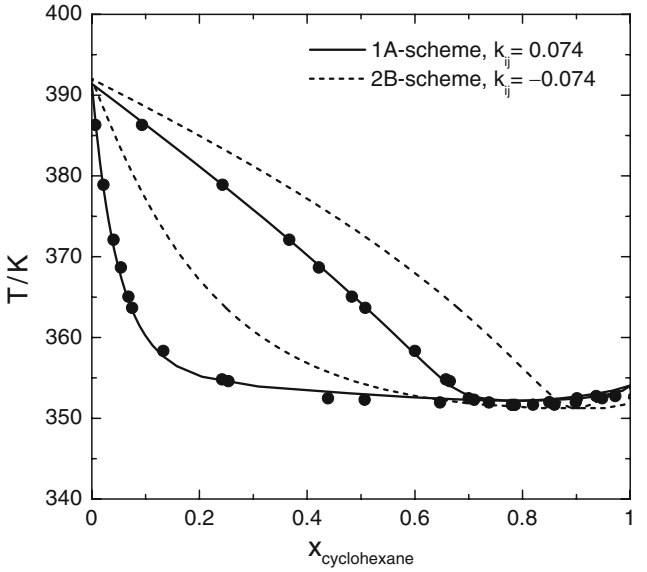

Fig. 12 Vapor–liquid equilibrium of the mixture cyclohexane/acetic acid at $p = 1\,\text{bar}$. *Dashed lines*: correlation results of PC-SAFT using the 2B-association scheme. *Solid lines*: PC-SAFT correlations considering using the 1A-association scheme. Experimental data taken from Miyamoto et al. [63]

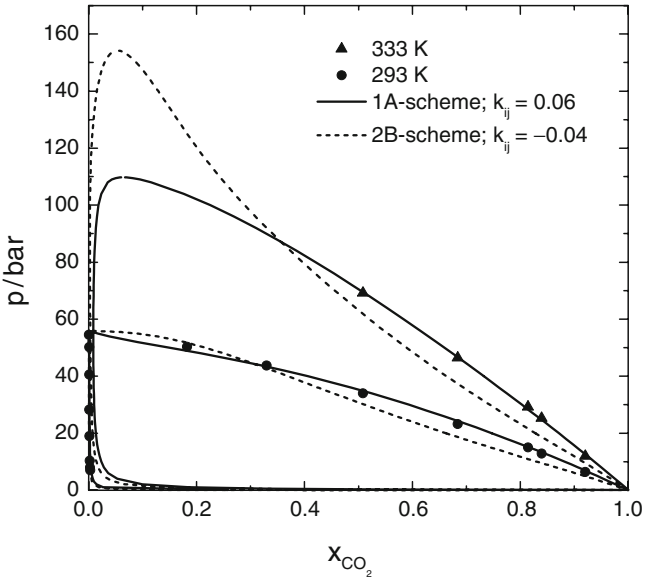

Fig. 13 Vapor–liquid equilibrium of the acetic acid/CO_2 mixture at two temperatures (*filled circles* for $T = 293.2\,\text{K}$, *filled triangles* for $T = 333.2\,\text{K}$). *Dashed lines*: correlations via PC-SAFT using the 2B-association scheme. *Solid lines*: PC-SAFT correlations using the 1A-association scheme. Experimental data are from Laugier et al. [64]

However, investigations have shown that accounting for the cross-association interactions have a minor influence on the phase behavior modeling and, thus, these interactions are not explicitly considered here. It can be seen that again the results using the 2B-association scheme for acetic acid cannot be brought into good agreement with experimental data, even using a binary interaction parameter k_{ij}. In the case of the 1A scheme, where the dimerization is considered, the correlation results are in excellent agreement with experimental data.

The mixture of acetic acid with ethyl acetate represents a system containing an associating and a polar compound in which induced association may occur, as described in the previous section. Modeling results for the vapor–liquid equilibrium of this mixture are presented in Fig. 14 using the 1A- and 2B-association schemes, respectively. It can be seen that the results are poorly represented using the 2B scheme, even applying a very high binary interaction parameter where the model calculates an azeotropic behavior. Again, the results are improved considerably when the dimerization is considered by the 1A scheme, even requiring a much smaller value for the binary interaction parameter k_{ij}.

It becomes obvious that the applied association scheme strongly affects the modeling results. Despite its simplicity, for carboxylic acids the 1A scheme leads to a reasonable description of mixture phase behavior containing compounds with different functionalities.

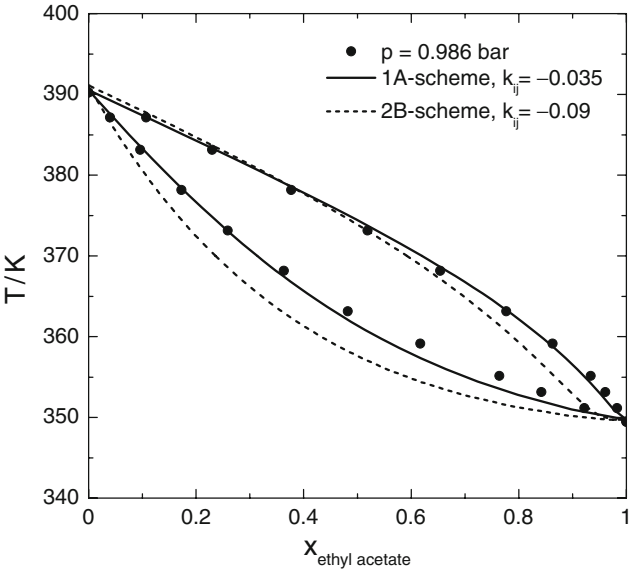

Fig. 14 Vapor–liquid equilibrium of the mixture acetic acid/ethyl acetate mixture at $p = 0.986$ bar. *Dashed lines*: correlations via PC-SAFT using the 2B-association scheme. *Solid lines*: PC-SAFT correlations using the 1A-association scheme. Experimental data are taken from Kato [65]

4 Modeling of Solid–Liquid Equilibria

PC-SAFT can also be applied to describe the solubility of solid solutes. This knowledge is particularly crucial for the study of crystallization, which is an important purification technique for many pharmaceutical and biological compounds.

Assuming pure solid phases, and neglecting the influence of the heat-capacity differences in the solid and liquid state, the solubility of a compound i at atmospheric pressure can be calculated as:

$$x_i^{\mathrm{L}} = \frac{\phi_{0i}^{\mathrm{L}}}{\phi_i^{\mathrm{L}}} \cdot \exp\left[-\frac{\Delta h_{0i}^{\mathrm{SL}}}{RT}\left(1 - \frac{T}{T_{0i}^{\mathrm{SL}}}\right)\right]. \tag{8}$$

Here, x_i^L represents the mole fraction of substance i in the liquid (L) phase. Δh_{0i}^{SL} and T_{0i}^{SL} are the enthalpy of melting and temperature of melting of pure substance i, respectively. They can be measured independently, e.g., using differential scanning calorimetry (DSC). In the case of compounds that decompose during melting (e.g., amino acids), the two pure-component properties can be treated as adjustable parameters [66]. The PC-SAFT model can be used to calculate the fugacity coefficients of substance i in the mixture (φ_i^L) and as pure component (φ_{0i}^L). The ratio of the fugacity coefficient in the mixture to the fugacity coefficient of pure component gives the activity coefficient γ_i^L.

To estimate the pure-component PC-SAFT parameters for solid solute compounds, binary solubility data in one solvent can be used since usually neither liquid-density nor vapor-pressure data of the pure solute are available.

The applicability of the PC-SAFT model to calculate and estimate organic-solute solubility is demonstrated here for the drug substance paracetamol which is commonly used for the relief of fever, headaches, and other minor aches and pains. There exist extensive sets of experimental solubility data for paracetamol in pure solvents and in solvent mixtures. The experimentally measured melting temperature of 441.2 K and the melting enthalpy of 26 kJ/mol from Manzo and Ahumada [67] were used for the solubility calculations. The original PC-SAFT model with association term was applied to calculate the solubility of paracetamol in different solvents and solvent mixtures. Paracetamol is modeled as an associating compound with two different types of association sites (A and B), each of them having two sites. Both types were assumed to be of equal strength. Hence, five pure-component parameters had to be determined for paracetamol: segment number, segment diameter, dispersion energy, association energy, and association volume. These parameters for paracetamol, as well as the binary parameter k_{ij} of paracetamol/water, were identified from its experimental solubility data in water from [68].

Using these parameters and the binary parameter k_{ij} for each paracetamol/solvent system, solubilities in other solvents such as acetone, ethanol, and toluene can also be modeled. The correlation results and the comparison to experimental data are shown in Fig. 15. The results reveal the ability of the PC-SAFT model to provide a description of the solubility of a complex molecule like paracetamol in different solvents that is remarkably consistent with the experiments.

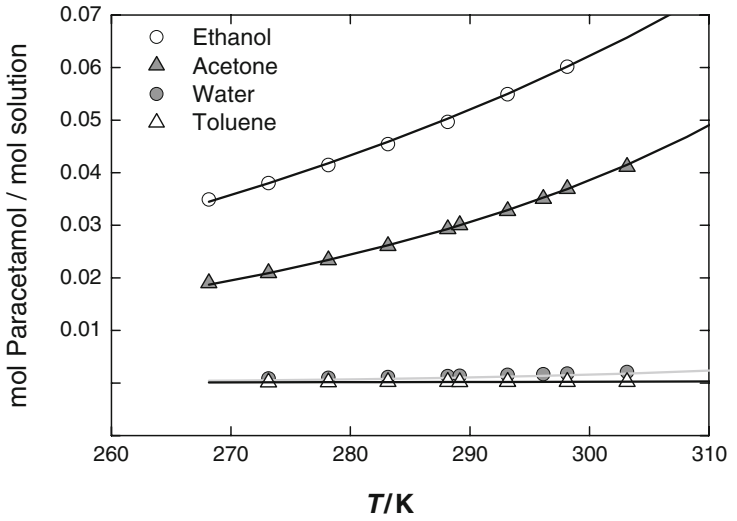

Fig. 15 Solubility of paracetamol in different pure solvents. *Symbols* are experimental data from [68]. *Solid lines* represent correlation results of PC-SAFT

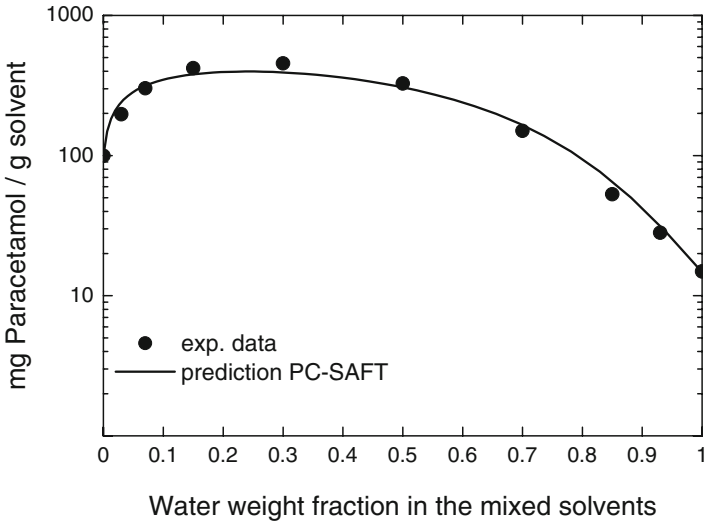

Fig. 16 Solubility of paracetamol in water/acetone mixtures of different compositions at 25°C. *Symbols* are experimental data from [69] and the *solid line* represents the model prediction with PC-SAFT

Based on the modeling of the solubility in pure solvents and the determined binary parameters, the solubility in mixed solvents can be predicted. Figure 16 shows the prediction results for the paracetamol solubility in a solution of water and acetone at 25°C as an example for a mixture of one polar and one hydrophilic solvent.

The experimental data exhibit a non-linear and non-monotonic solubility behavior. Starting from the binary system paracetamol/acetone (solubility about 100 mg paracetamol/g acetone) the solubility increases extremely as a small amount of water is added (up to 450 mg paracetamol/g mixed solvent at a water weight fraction of 0.3 in the solvent mixture). This happens although paracetamol is much less soluble in pure water (about 15 mg/g water) than in acetone. PC-SAFT predicts this behavior without fitting any parameters to the ternary mixture, as shown in Fig. 16.

The non-linear and non-monotonic behavior is also observed for the solubility of adipic acid in solvent mixtures of 1-propanol and 1,4-dioxane at different temperatures in the range 25–60°C. 1-propanol is a much worse solvent for adipic acid than 1,4-dioxane. Nevertheless, adding of 1-propanol to 1,4-dioxane up to a concentration of about 25% enhances the adipic-acid solubility, which is also predicted by PC-SAFT, as depicted in Fig. 17. A further increasing amount of 1-propanol, however, results in the decline of the adipic acid solubility, which is again also predicted by PC-SAFT. Given that the adipic acid solubilities in the mixed solvents are predicted using the parameters identified from solubility data in the pure solvents, the results for adipic-acid solubility are considered to be very satisfactory.

To account for pH effects on the solubility of, e.g., amino acids in water, a simple approach can be applied, as proposed by Gupta and Heidemann [70], using the pK_a values of the respective amino acids to calculate the solubility at different pH:

$$x_i^{\mathrm{L}} = x_{i,\,\mathrm{isoelectric}}^{\mathrm{L}} \cdot \left(1 + \frac{10^{-\mathrm{pH}}}{K_{a1}} + \frac{K_{a2}}{10^{-\mathrm{pH}}}\right). \tag{9}$$

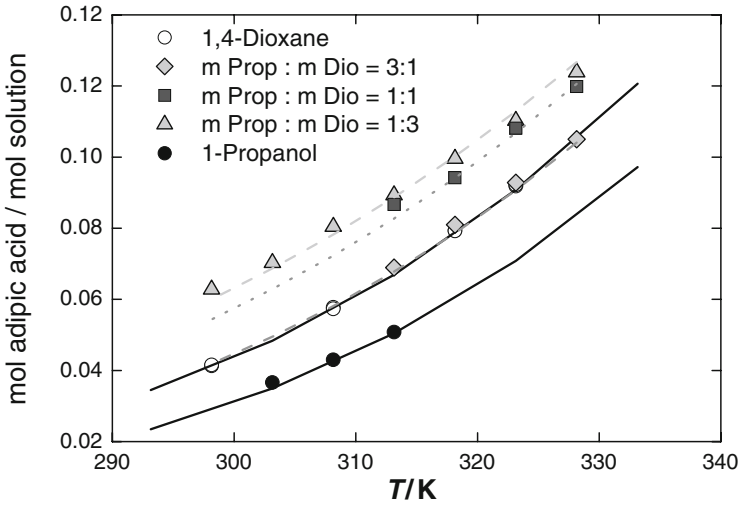

Fig. 17 Solubility of adipic acid in 1-propanol, 1,4-dioxane, and in mixtures of 1-propanol and 1,4-dioxane. *Solid lines* are modeling results using PC-SAFT. *Dashed lines* are PC-SAFT predictions

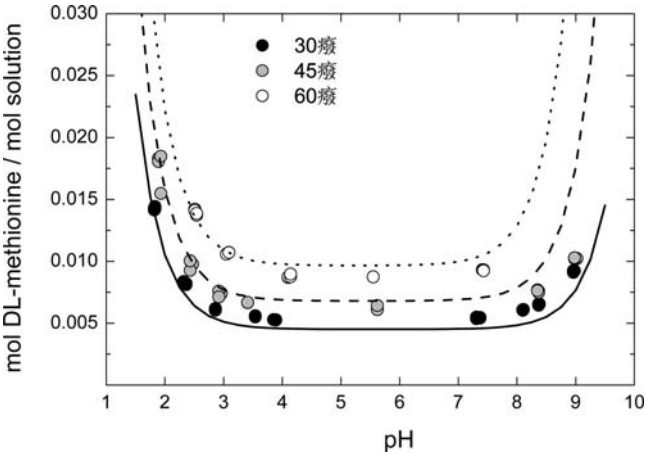

Fig. 18 Solubility of DL-methionine in aqueous solutions as a function of pH values. *Symbols* represent experimental data from [66], and *lines* represent PC-SAFT calculation results

The solubility at the isoelectric point $x_i^{\mathrm{L},\ \mathrm{isoelectric}}$ at different temperatures can be calculated using PC-SAFT according to Eq. 8. In Fig. 18 the experimental data and calculation results for the solubility of the amino acid DL-methionine at three different temperatures and altered pH values are presented [66]. Using the pK_a values of DL-methionine, the calculation results of the solubility in HCl/NaOH solutions show good agreement in the isoelectrical band and also in basic and acidic environments.

Considering solid–liquid equilibria, melting systems can show solid complexes, which are formed due to strong hydrogen-bonding interactions between the participating species. Such complexes are often referred to as intermolecular compounds, adducts (or addition compounds), hydrates (in aqueous systems), or solvates (in non-aqueous systems). These complexes usually exist only in the solid phase. To describe the solubility of such hydrates and solvates, the complex formation can be treated like a chemical reaction between the liquid species (e.g., A and B) and described by the corresponding equilibrium constants [71]:

$$|\nu_A| A^{(L)} + |\nu_B| B^{(L)} \Leftrightarrow A_{|\nu_A|} B_{|\nu_B|}{}^{(S)}. \tag{10}$$

Assuming again a pure solid complex, the equilibrium constant for the reaction in Eq. 10 can be expressed as a function of liquid concentrations and activity coefficients according to:

$$K_a = \prod_i a_i^{\nu_i} = (x_A \gamma_A)^{\nu_A} (x_B \gamma_B)^{\nu_B}. \tag{11}$$

Here, the activity coefficient of component A and B, respectively, can again be calculated as the ratio of the fugacity coefficient of the component in the mixture and the fugacity coefficient of the pure component, both of which are again calculated with PC-SAFT.

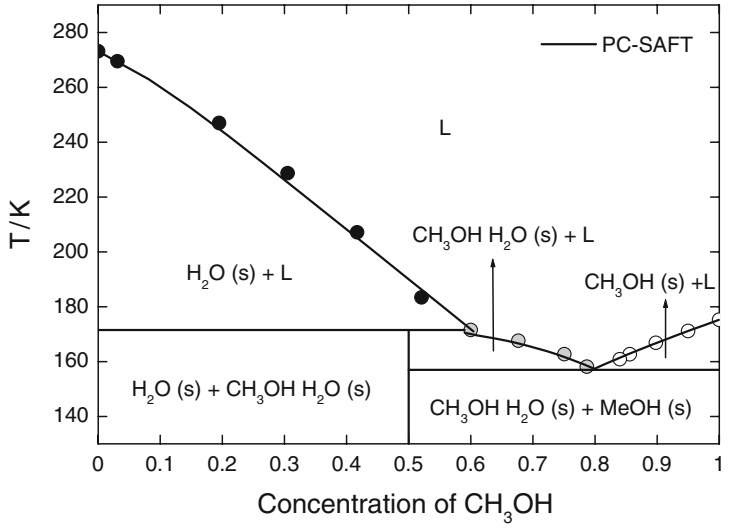

Fig. 19 Melting phase diagram of methanol/water with monohydrate formation. *Symbols* are experimental data from [72, 73]. *Solid lines* are calculation results of PC-SAFT

The equilibrium constant K_a is determined using the pseudo-melting properties of the solid complex as described in [71]. To calculate the solubility of the solid complex, Eq. 11 has to be solved iteratively.

Figure 19 illustrates the power of this approach to describing solid–liquid equilibria with solid-complex formation for the example methanol–water. In addition to the crystallization of pure methanol and of pure water, this system forms a 1:1 complex [methanol monohydrate $CH_3OH \cdot H_2O(s)$]. The various phase regions are indicated in the phase diagram. The calculated lines characterize the phase boundaries of solid–liquid and solid–solid equilibrium. The type of solid (either pure component or complex) is also identified. As can be seen, using the same set of parameters to calculate the solubility of the two pure components methanol and water, the crystallization curve of the monohydrate could also be modeled in a very good agreement with experimental data.

The excellent match with experiments is also confirmed for the ternary system bisphenol A (BPA)/phenol/water, as depicted in Fig. 20 for a water concentration of 30 mol%. In this system, BPA and phenol form a solid 1:1 complex. The symbols represent the literature data from Kwok et al. [74] and the lines are calculation results using PC-SAFT for the solubilities of pure BPA, pure phenol, and BPA/phenol complex. Again, PC-SAFT is able to describe the solubility of pure solids and of solid complex in a very good agreement with the experimental data.

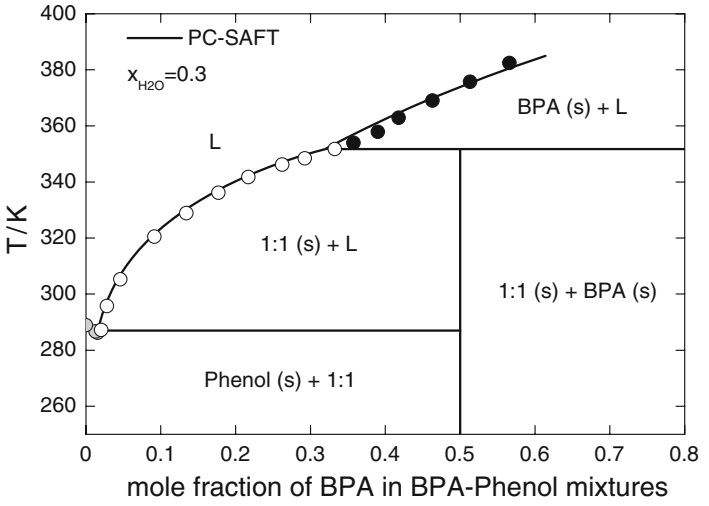

Fig. 20 Phase diagram of the ternary BPA/phenol/water system at a water concentration of 30 mol%. Comparison of experimental data (*symbols*) from [74] with modeling results using PC-SAFT (*lines*)

5 Polymer Systems

Due to the large differences in molecular size of polymers and solvents, and due to the molar-mass distribution of a polymer, modeling of polymer systems is always challenging. The PC-SAFT model is based on the hard-chain reference system and thus explicitly considers the attractive interactions of chain molecules instead of those of the unbonded segments. Therefore, PC-SAFT is particularly suitable for describing polymer systems [19, 61, 75–84].

Compared to low molecular weight substances, the determination of pure-component parameters for polymers is more difficult because polymer vapor-pressure data are not accessible. A methodology for the identification of pure-component parameters for polymers is the simultaneous fitting of liquid densities and phase-equilibrium data of one binary system [19, 76]. It has been shown in many applications that the so-determined pure-component parameters are suitable for different mixtures and can thus be regarded as characteristic for a specific polymer. For example, the pure-component parameters for low-density polyethylene (LDPE) were determined by fitting the liquid densities of LDPE and the experimental binary data of LDPE/ethene. The same pure-component parameters of LDPE were then subsequently used to model the cloud points of 5 wt.% LDPE in different solvents (ethane, propane, propene, 1-butene, and *n*-butane) using one k_{ij} for each respective binary system [85]. The correlation results and the comparison to the experimental data from [86] are depicted in a pressure–temperature diagram in Fig. 21, which shows on the one hand the good agreement between the modeling results and experimen-

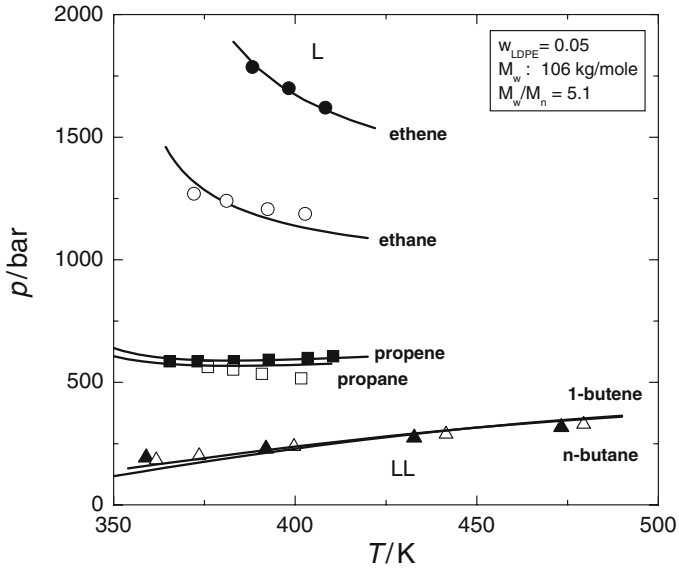

Fig. 21 High-pressure equilibrium for mixtures of low-density polyethylene (LDPE) with varying solvents: ethene, ethane, propene, propane, 1-butene, and *n*-butane. Comparison of experimental cloud-point measurements [86] to calculation results of the PC-SAFT equation of state. (LDPE-1-butene *open triangles*)

tal data and proves on the other hand the applicability of the described method for determination of the pure-component parameters of polymers.

Furthermore, the influence of molecular weight on phase behavior can be taken into account when applying PC-SAFT. By only varying the segment number proportional to the molecular weight, the solubility of various polyethylene samples in ethene can be predicted by PC-SAFT, as presented in Fig. 22 for four molecular weights ranging from 19 to 129 kg/mol.

The phase behavior of copolymers is influenced by the nature of the different monomers as well as by the monomer composition within the copolymer backbone. An extension of the PC-SAFT equation of state to heterosegment molecules also allows the composition of the different monomers in the copolymer chain to be accounted for and, to a certain extent, the arrangement of the monomers also [85]. The underlying molecular model of a copolymer consisting of α-segments and β-segments is shown in Fig. 23. The modeling of a copolymer–solvent mixture requires the appropriate pure-component parameters of the respective homopolymer segments and of the solvent. The binary parameters of the homopolymer–solvent systems ($k_{\alpha-S}$, $k_{\beta-S}$) can be determined from fitting the phase equilibrium data of the respective homopolymers/solvent systems. To describe the copolymer system, if necessary, one additional binary interaction parameter can be fitted to binary copolymer data, which accounts for the dispersive interactions between the unlike homopolymer segments ($k_{\alpha-\beta}$) in the copolymer solution.

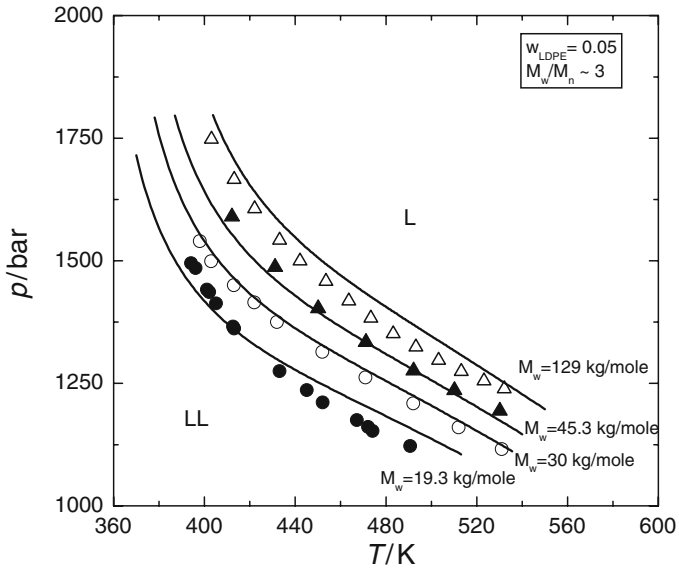

Fig. 22 Experimental cloud-point data (*symbols*) of polyethylene samples with different molecular weights [87] compared to the prediction results using PC-SAFT (*lines*)

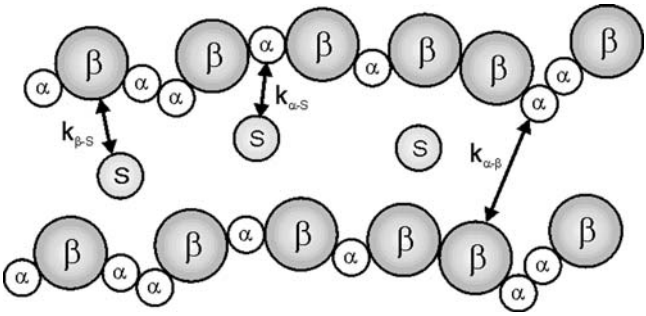

Fig. 23 Molecular model for a copolymer of type poly(α-*co*-β), composed of segments α and β in interaction with a solvent S. There exist three types of interactions α-β, α-S, as well as β-S, which are described by three binary interaction parameters

Applications of the PC-SAFT equation of state to polyolefin copolymers [85], branched polyolefins [80], copolymers and terpolymers of ethylene, and carboxylic acid esters [76, 78, 88] revealed the strength of this methodology.

This is illustrated in Fig. 24 for the solubility of poly(ethylene-*co*-ethyl acrylate) [poly(E-*co*-EA)] in ethene, which compares experimental cloud-point-pressure data to modeling results of PC-SAFT. Starting from the homopolymer polyethylene, an increasing ethyl-acrylate content in the copolymer backbone first leads to an increasing solubility of the poly(E-*co*-EA) copolymers and thus to lower cloud-point pressures. After passing through a minimum at an EA content of about 30 mol% in the polymer backbone, the solubility again decreases with rising EA content.

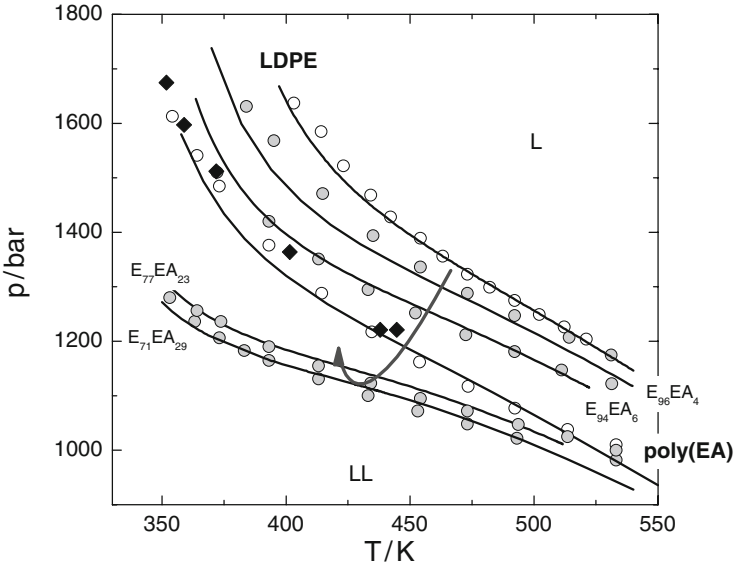

Fig. 24 Cloud-point pressure curves for mixtures of ethene and poly(E-*co*-EA) for various monomer compositions. Comparison of experimental data (*symbols*) from Lora et al. [89] and calculations obtained with the PC–SAFT model (*lines*). Indices give the ethylene and ethyl-acrylate compositions (mol%) in the copolymer molecules, respectively

The remarkably good agreement of experimental data and the PC-SAFT calculations for the different copolymer/solvent mixtures is obtained using only the information of homopolymer systems as well as one additional binary interaction parameter $k_{\alpha\beta}$. However, even without fitting the binary parameter $k_{\alpha\beta}$, PC-SAFT did qualitatively predict the non-monotonic solubility behavior. None of the parameters is dependent on temperature or copolymer composition. Thus, PC-SAFT allows for the estimation and, to a certain extent, even predicts the cloud-point behavior of copolymer systems for a wide range of pressures, temperatures, and copolymer compositions.

The parameter identification for copolymer systems might be challenging if experimental data for the respective homopolymers is scarce or not available. This is the case, e.g., for methacrylic acid copolymers where no experimental phase-equilibrium data for the homopolymer poly(methacrylic acid) [poly(MAA)] in any solvent is available. Poly(ethylene-*co*-methacrylic acid) [poly(E-*co*-MAA)] is an example of a copolymer that consists of one non-polar-monomer group (ethylene) and one associating monomer group (methacrylic acid). The methacrylic acid (MAA) content in the copolymers in Fig. 25 varies from 1% to 10.3 mol% and the copolymer molecular weights M_w range from 32 to 63 kg/mol, with a polydispersity index of about 3.3. To characterize the homopolymer poly(MAA), five pure-component parameters are required. These parameters can be determined from fitting the cloud-point data of one copolymer/solvent system,

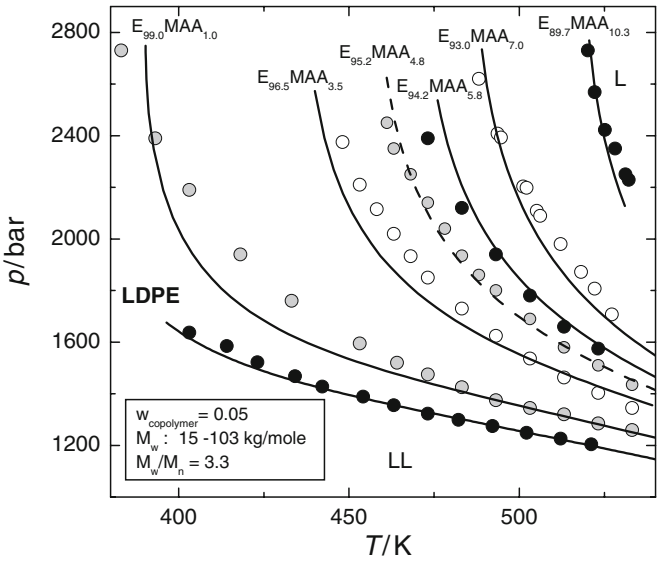

Fig. 25 Cloud-point pressure curves for mixtures of ethene and poly(E-*co*-MAA). The dashed line represents correlation results from the parameter determination of PC-SAFT. Experimental data taken from Buback and Latz [90] (*circles*) are compared with PC-SAFT predictions (*solid lines*). *Indices* give the ethylene and methacrylic-acid content (mol%) in the copolymer samples

e.g., poly($E_{95.2}-co$-$MAA_{4.8}$)/ethene. Moreover, the polydispersity of the polymers has also a profound effect on the phase behavior. To account for that, the polydisperse poly(E-*co*-MMA) copolymers were characterized by two representative pseudo-components [61]. Using that approach, the solubility of a whole series of these copolymers having different comonomer compositions and molecular weights could be predicted in very satisfactory agreement with the experimental cloud-point pressures. This demonstrates that reasonable model parameters can be obtained for complex polymeric systems, even if experimental data for the homopolymers is scare or not available.

When the parameters of the homopolymers as well as the required binary parameters are known, even more complex polymers (e.g., terpolymers) can be modeled. Figure 26 shows the cloud-point pressure curves for terpolymers that consist of monomers that have very different functionalities: the non-polar ethylene, the polar butyl methacrylate (BMA), and the associating monomer methacrylic acid, poly(E-*co*-BMA-*co*-MAA). The solvent is again ethene. The lines represent pure predictions of the phase behavior using the PC-SAFT parameters obtained for the binary homopolymer/ethene systems and the respective copolymer/ethene systems without any additional parameter fitting or readjustment. It can be seen that the experimentally observed effects of the terpolymer composition on solubility are well predicted by the PC-SAFT model.

Finally, the influence of cosolvents can also be predicted by PC-SAFT. Figure 27 illustrates a typical example of a mixture that consists of the copolymer

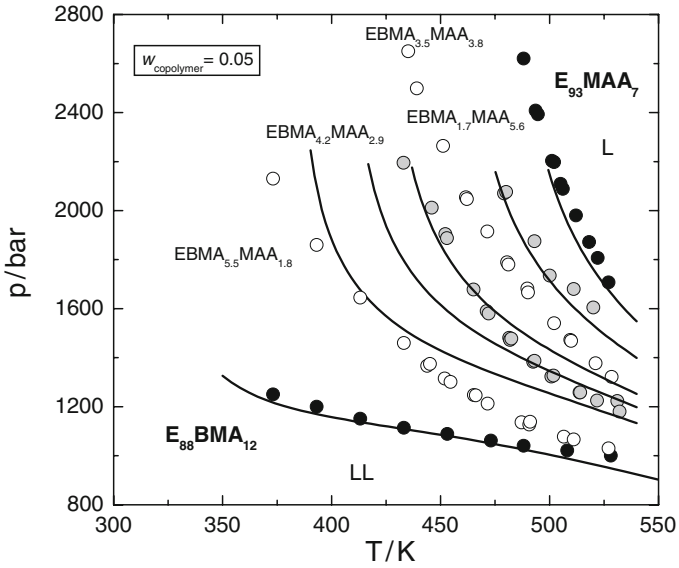

Fig. 26 Cloud-point pressure curves for the copolymers poly(E-*co*-BMA) and poly(E-*co*-MAA), as well as for the terpolymers poly(E-*co*-BMA-*co*-MAA) in ethene. Comparison of experimental data from [61, 78, 90] and predictions obtained by PC-SAFT

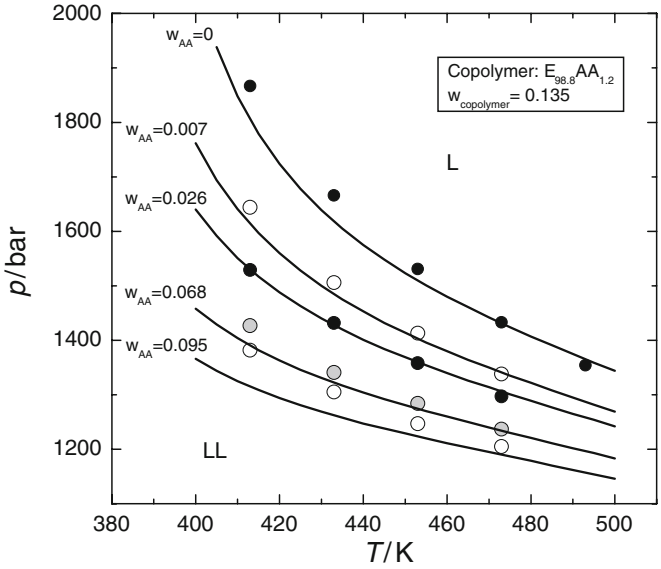

Fig. 27 Influence of acrylic acid (AA) on the cloud-point pressures of poly(ethylene-*co*-acrylic acid) in ethene**.** Ethylene content in the copolymer backbone is 98.9%. w_{AA} denotes the acrylic-acid weight fraction in the polymer-free system. Experimental data from Wind [91] (*symbols*) are compared with predictions via PC-SAFT (*solid lines*)

poly(ethene-*co*-acrylic acid) (EAA), ethene and different concentrations of the cosolvent acrylic acid (AA). Although all model parameters were previously determined from pure-component and binary data, the influence of the cosolvent is adequately predicted by PC-SAFT. Again, all parameters used are independent of temperature and concentration. The very good agreement of the experimental data and the predictions demonstrate that the PC-SAFT model is also capable of almost quantitatively predicting the influence of a cosolvent/comonomer on polymer solubility.

6 Summary

State-of-the-art thermodynamic models have a sound physical basis. As shown for the PC-SAFT equation of state they can be successfully applied to a whole variety of substances ranging from small gas molecules up to organic solvents and polymeric systems. Recent developments and modifications further extended the physical basis by explicitly accounting for complex intermolecular interactions such as association, polar interactions, and induced interactions that only occur in mixtures but not in the pure components. These achievements ensured a remarkably improved ability of the models to correlate and even to predict thermodynamic properties of very asymmetric and complex mixtures over a wide range of component properties and system conditions.

References

1. Chapman WG, Gubbins KE, Jackson G,Radosz M (1989) Fluid Phase Equilibr 52:31
2. Chapman WG, Gubbins KE, Jackson G, Radosz M (1990) Ind Eng Chem Res 29:1709
3. Huang SH, Radosz M (1990) Ind Eng Chem Res 29:2284
4. Huang SH, Radosz M (1991) Ind Eng Chem Res 30:1994
5. Carnahan NF, Starling KE (1969) J Chem Phys 51:635
6. Alder BJ, Young DA, Marx MA (1972) J Chem Phys 56:3013
7. Chen SS, Kreglewski A (1977) Ber Bunsen Phys Chem 81:1048
8. Wertheim MS (1987) J Chem Phys 87:7323
9. Song YH, Lambert SM, Prausnitz JM (1994) 10. Ind Eng Chem Res 33:1047
10. Chang J, Sandler SI (1994) Mol Phys 81:745
11. Gil-Villegas A, Galindo A, Whitehead PJ, Mills SJ, Jackson G, Burgess AN (1997) J Chem Phys 106:4168
12. Hino T, Prausnitz JM (1997) Fluid Phase Equilib 138:105
13. Banaszak M, Chiew YC, Radosz M (1993) Phys Rev E 48:3760
14. Tavares FW, Chang J, Sandler SI (1997) Fluid Phase Equilibr 140:129
15. Chapman WG (1990) J Chem Phys 93:4299
16. Muller EA, Vega LF, Gubbins KE (1994) Mol Phys 83:1209
17. Blas FJ, Vega LF (1997) Mol Phys 92:135
18. Gross J, Sadowski G (2001) Ind Eng Chem Res 40:1244
19. Gross J, Sadowski G (2002) Ind Eng Chem Res 41:1084
20. Gross J, Sadowski G (2002) Ind Eng Chem Res 41:5510
21. Tumakaka F, Sadowski G (2004) Fluid Phase Equilib 217:233

22. Muller EA, Gubbins KE (2001) Ind Eng Chem Res 40:2193
23. Gubbins KE, Gray CG (1972) Mol Phys 23:187
24. Cotterman RL, Prausnitz JM (1986) AIChE J 32:1787
25. Cotterman RL, Prausnitz JM (1986) AIChE J 32:1799
26. Walsh JM, Jin G, Donohue MD (1991) Fluid Phase Equilibr 65:209
27. Kraska T, Gubbins KE (1996) Ind Eng Chem Res 35:4727
28. Kraska T, Gubbins KE (1996) Ind Eng Chem Res 35:4738
29. Xu K, Li Y, Liu W (1998) 142:55
30. Tang Y, Wang Z, Lu BY (2001) Mol Phys 99:65
31. Sear RP (1996) Phys Rev Lett 76:2310
32. Jog PK, Chapman WG (1999) Mol Phys 97:307
33. Gross J, Vrabec J (2006) AIChE J 52:1194
34. Saager B, Fischer J (1992) Fluid Phase Equilibr 72:67
35. Saager B, Fischer J, Neumann M (1991) Molec Simul 6:27
36. Kleiner M, Gross J (2006) AIChE J 52:1951
37. Wertheim M (1977) Mol Phys 34:1109
38. Wertheim M (1979) Mol Phys 37:83
39. Cameretti LF, Sadowski G, Mollerup JM (2005) Ind Eng Chem Res 44:3355
40. Cameretti LF, Sadowski G (2007) Chem Eng Proc 47:1018
41. Chapman WG, Jackson G, Gubbins KE (1988) Mol Phys 65:1057
42. Wertheim MS (1984) J Stat Phys 35:19
43. Wertheim MS (1984) J Stat Phys 35:35
44. Wertheim MS (1986) J Chem Phys 85:2929
45. Barker JA, Henderson D (1967) J Chem Phys 47:2856
46. Barker JA, Henderson D (1967) J Chem Phys 47:4714
47. Wolbach JP, Sandler IS (1998) Ind Eng Chem Res 37:2917
48. Shen SB, Wang YR, Shi J, Benson GC, Lu BCY (1990) J Chem Thermodyn 22:387
49. Mcglashan M, Morcom KW (1961) T Faraday Soc 57:581
50. Holleman T (1965) Physica 31:49
51. Wilding WV, Wilson LC, Wilson GM (1987) Fluid Phase Equilibr 36:67
52. Artal M, Embid JM, Marras G, Velasco I, Otin S (1995) J Chem Eng Data 40:1154
53. Akamatsu Y, Ogawa H, Murakami S (1987) Thermochim Acta 113:141
54. Kleiner M, Sadowski G (2007) J Phys Chem C 111:15544
55. Danov SM, Obmelyukhina TN, Chubarov GA, Balashov AL, Dolgopolov AA (1990) J Appl Chem USSR 63:566
56. Frolova EA, Ershova TP, Stepanova VA, Pavlov SY (1979) Osnov Organ Sintez i Neftekhimiya 11:90
57. Fu J, Wang K, Hu Y (1988) J Chem Ind Eng China 39:64
58. Lloyd BA, Thompson SO, Ferguson JB (1937) Can J Research 15B:98
59. Clausse D, Lambert JP, Guigon P, Boudehen-Boiveaut A (1988) Calorim Anal Therm 19: C21.1
60. Chubarov GA, Danov SM, Brovkina GV, Kupriyanov TV (1978) J Appl Chem USSR 51:434
61. Kleiner M, Tumakaka F, Sadowski G, Latz H, Buback M (2006) Fluid Phase Equilibr 241:113
62. Weltner W (1955) J Am Chem Soc 77:3941
63. Miyamoto S, Nakamura S, Iwai Y, Arai Y (2000) J Chem Eng Data 45:857
64. Laugier S, Richon D, Renon H (1990) Fluid Phase Equilibr 54:19
65. Kato M (1988) J Chem Eng Data 33:499
66. Fuchs D, Fischer J, Tumakaka F, Sadowski G (2006) Ind Eng Chem Res 45:6578
67. Manzo RH, Ahumada AA (1990) J Pharm Sci 79:1109
68. Granberg RA, Rasmuson AC (1999) J Chem Eng Data 44:1391
69. Granberg RA, Rasmuson AC (2000) J Chem Eng Data 45:478
70. Gupta RB, Heidemann RA (1990) AIChE J 36:333
71. Tumakaka F, Prikhodko IV, Sadowski G (2007) Fluid Phase Equilibr 260:98
72. Miller GA, Carpenter DK (1964) J Chem Eng Data 9:371
73. Ott JB, Goates JR, Waite BA (1979) J Chem Thermodyn 11:739

74. Kwok KS, Chan HC, Chan CK, Ng KM (2005) Ind Eng Chem Res 44:3788
75. Cheluget EL, Bokis CP, Wardhaugh L, Chen CC, Fisher J (2002) Ind Eng Chem Res. 41:968
76. Tumakaka F, Gross J, Sadowski G (2002) Fluid Phase Equilibr 194:541
77. Lindvig T, Michelsen ML, Kontogeorgis GM (2004) Ind Eng Chem Res 43:1125
78. Becker F, Buback M, Latz H, Sadowski G, Tumakaka F (2004) Fluid Phase Equilibr 215:263
79. Arce P, Aznar M (2005) Fluid Phase Equilibr 238:242
80. Dominik A, Chapman WG (2005) Macromolecules 38:10836
81. van Schilt MA, Wering RM, van Meerendonk WJ, Kemmere MF, Keurentjes JTF, Kleiner M, Sadowski G, de Loos TW (2005) Ind Eng Chem Res 44:3363
82. Hungenberg KD, Nieken U, Zollner K, Gao J, Szekely A (2005) Ind Eng Chem Res 44:2518
83. Spyriouni T, Economou IG (2005) Polymer 46:10772
84. Arce P, Mattedi S, Aznar M (2006) Fluid Phase Equilibr 246:52
85. Gross J, Spuhl O, Tumakaka F, Sadowski G (2003) Ind Eng Chem Res 42:1266
86. Hasch BM, Lee SH, McHugh MA (1996) J Appl Polym Sci 59:1107
87. Latz H (2004) Kinetische und thermodynamische Untersuchungen der Hochdruck-Copolymerisation von Ethen mit (Meth)Acrylsäureestern. Georg-August-Universität zu Göttingen, Göttingen
88. Tumakaka F, Sadowski G, Latz H, Buback M (2007) J Supercrit Fluid 41:461
89. Lora M, Rindfleisch F, McHugh MA (1999) J Appl Polym Sci 73:1979
90. Buback M, Latz H (2003) Macromol Chem Physic 204:638
91. Wind RW (1992) Untersuchungen zum Phasenverhalten von Mischungen aus Ethylen, Acrylsäure und Ethylen-Acrylsäure-Copolymeren unter hohem Druck. TH Darmstadt, Darmstadt

Appendix

This section provides a summary of the equation of state contributions to the residual Helmholtz energy according to PC-SAFT (Eq. 3).

Hard-Chain Reference Contribution

The Helmholtz energy of the hard-chain reference term is given as:

$$\frac{A^{\mathrm{hc}}}{NkT} = \bar{m} \cdot \frac{A^{\mathrm{hs}}}{N_s kT} - \sum_i x_i (m_i - 1) \cdot \ln g_{ii}^{\mathrm{hs}}(d_{ii}), \tag{12}$$

where x_i is the mole fraction of chains of component i, m_i is the number of segments in a chain and the mean segment number in the mixture is defined as:

$$\bar{m} = \sum_i x_i m_i. \tag{13}$$

The Helmholtz energy for the hard-sphere segments A^{hs}/NkT in Equ. 12 is given on a per-segment basis as:

$$\frac{A^{\mathrm{hs}}}{N_s kT} = \frac{1}{\zeta_0}\left[\frac{3\zeta_1\zeta_2}{(1-\zeta_3)} + \frac{\zeta_2^3}{\zeta_3(1-\zeta_3)^2} + \left(\frac{\zeta_2^3}{\zeta_3^2} - \zeta_0\right) \cdot \ln(1-\zeta_3)\right], \tag{14}$$

where N_s is related to the number of hard-spheres, the radial pair distribution function for the hard-sphere fluid is given by:

$$g_{ij}^{\mathrm{hs}}(d_{ij}) = \frac{1}{(1-\zeta_3)} + \left(\frac{d_i d_j}{d_i + d_j}\right)\frac{3\zeta_2}{(1-\zeta_3)^2} + \left(\frac{d_i d_j}{d_i + d_j}\right)^2 \frac{2\zeta_2^2}{(1-\zeta_3)^3}, \tag{15}$$

and ζ_n is defined as:

$$\zeta_n = \frac{\pi}{6}\cdot\rho\sum_i x_i m_i d_i^n \qquad n = \{0,1,2,3\}. \tag{16}$$

The temperature-dependent segment diameter is obtained as:

$$d_i = \sigma_i\left(1 - 0.12\cdot\exp\left(-3\cdot\frac{\varepsilon_i}{kT}\right)\right), \tag{17}$$

where σ_i is the temperature-independent segment diameter and ε_i/k is the depth of the pair-potential.

Dispersion Contribution

The dispersion contribution to the Helmholtz energy is given by:

$$\begin{aligned}\frac{A^{\mathrm{disp}}}{NkT} &= -2\pi\rho\cdot I_1(\eta,\bar{m})\cdot\sum_i\sum_j x_i x_j m_i m_j\left(\frac{\varepsilon_{ij}}{kT}\right)\sigma_{ij}^3 \\ &-\pi\rho\cdot\bar{m}\cdot C_1\cdot I_2(\eta,\bar{m})\cdot\sum_i\sum_j x_i x_j m_i m_j\left(\frac{\varepsilon_{ij}}{kT}\right)^2\sigma_{ij}^3\end{aligned} \tag{18}$$

with

$$\begin{aligned}C_1 &= \left(1 + Z^{hc} + \rho\frac{\partial Z^{hc}}{\partial\rho}\right)^{-1} \\ &= \left(1 + \bar{m}\frac{8\eta - 2\eta^2}{(1-\eta)^4} + (1-\bar{m})\frac{20\eta - 27\eta^2 + 12\eta^3 - 2\eta^4}{[(1-\eta)(2-\eta)]^2}\right)^{-1}.\end{aligned} \tag{19}$$

The power series I_1 and I_2 depend only on density and segment number according to:

$$I_1(\eta,\bar{m}) = \sum_{i=0}^{6} a_i(\bar{m})\cdot\eta^i, \tag{20}$$

$$I_2(\eta,\bar{m}) = \sum_{i=0}^{6} b_i(\bar{m})\cdot\eta^i, \tag{21}$$

where the coefficients $a_i(m)$ and $b_i(m)$ are functions of the segment number:

$$a_i(\bar{m}) = a_{0i} + \frac{\bar{m}-1}{\bar{m}} a_{1i} + \frac{\bar{m}-1}{\bar{m}} \frac{\bar{m}-2}{\bar{m}} a_{2i}, \tag{22}$$

$$b_i(\bar{m}) = b_{0i} + \frac{\bar{m}-1}{\bar{m}} b_{1i} + \frac{\bar{m}-1}{\bar{m}} \frac{\bar{m}-2}{\bar{m}} b_{2i}. \tag{23}$$

The universal model constants in Eqs. 22 and 23 are given in the work of Gross and Sadowski [18].

Association Contribution

The association contribution to the Helmholtz energy is given as:

$$\frac{A^{\text{assoc}}}{NkT} = \sum_i x_i \sum_{\mathrm{A}_i=1}^{n\text{site}} \left(\ln X^{\mathrm{A}_i} - \frac{X^{\mathrm{A}_i}}{2} + \frac{1}{2} \right). \tag{24}$$

It is important to note that the summation runs over all association sites of the molecule i where X^{A_i} is the fraction of the free molecules i that are not bonded at the association site A:

$$X^{\mathrm{A}_i} = \left(1 + \rho \cdot \sum_j x_j \sum_{\mathrm{B}_j}^{n\text{sites}} X^{\mathrm{B}_j} \cdot \Delta^{\mathrm{A}_i \mathrm{B}_j} \right)^{-1} \tag{25}$$

with

$$\Delta^{\mathrm{A_j B_j}} = g_{ij}^{\mathrm{hs}}(d_{ij}) \cdot \kappa^{\mathrm{A_i B_j}} \cdot \sigma_{\mathrm{ij}}^3 \left(\exp\left(\frac{\varepsilon^{\mathrm{A_i B_j}}}{kT} \right) - 1 \right), \tag{26}$$

where $g_{\mathrm{ij}}^{\mathrm{hs}}(d_{\mathrm{ij}})$ is the pair distribution function of hard spheres given in Eq. 15.

Dipolar Contribution

The Helmholtz energy contribution from dipolar interactions of induced dipoles is given as:

$$\frac{A^{\text{dipole}}}{NkT} = \frac{A'^{\text{dipole}}}{NkT} + \frac{1}{2} kT \sum_{\mathrm{i}} x_{\mathrm{i}} \alpha_{\mathrm{i}} \left(\frac{1}{x_{\mathrm{i}}} \frac{\partial}{\partial \mu_{\mathrm{i}}^{\mathrm{eff}}} \left(\frac{A'^{\text{dipole}}}{NkT} \right) \right)_{\rho,T}^2, \tag{27}$$

where α_i is the molecular polarizability and the term A'^{dipole}/NkT is defined as:

$$\frac{A'^{\text{dipole}}}{NkT} = \left(\frac{A_2'}{NkT} \left[1 - \frac{A_3'}{A_2'} \right]^{-1} \right). \tag{28}$$

The first-order and second-order perturbation terms in Eq. 28 are given as:

$$\frac{A_2'}{NkT} = -\pi \frac{\rho}{(kT)^2} \sum_{\mathrm{i}} \sum_{\mathrm{j}} x_{\mathrm{i}} x_{\mathrm{j}} \frac{\left(z_i^{\mathrm{A}} z_j^{\mathrm{A}} - z_i^{\mathrm{B}} z_j^{\mathrm{B}} \right)}{\sigma_{\mathrm{ij}}^3} \frac{n_{\mu,i}}{m_i} \frac{n_{\mu,j}}{m_j} J_{2,ij}^{DD}, \tag{29}$$

$$\frac{A_3'}{NkT} = -\frac{4}{3}\pi^2 \frac{\rho^2}{(kT)^3} \sum_i \sum_j \sum_k x_i x_j x_k \frac{\left(z_i^{\mathrm{A}} z_j^{\mathrm{A}} z_k^{\mathrm{A}} - z_i^{\mathrm{B}} z_j^{\mathrm{B}} z_k^{\mathrm{B}} \right)}{\sigma_{ij}\sigma_{ik}\sigma_{jk}} \frac{n_{\mu,i}}{m_i} \frac{n_{\mu,j}}{m_j} \frac{n_{\mu,k}}{m_k} J_{3,ijk}^{DD}, \tag{30}$$

where $n_{\mu,i}$ is the number of dipolar segments in the molecule and z_i^A and z_i^B are defined as:

$$z_{\mathrm{i}}^{\mathrm{A}} = (\mu_i^{\mathrm{eff}})^2 + 3\,kT\,\alpha_i, \tag{31}$$

$$z_i^B = 3\,kT\,\alpha_i. \tag{32}$$

In Eqs. 29 and 30, the expressions $J_{2,ij}^{DD}$ and $J_{3,ijk}^{DD}$ are given by simple power functions of the dimensionless density η as:

$$J_{2,ij}^{DD} = \sum_{n=0}^{4} \left(a_{n,ij} + b_{n,ij} \frac{\varepsilon_{ij}}{kT} \right) \eta^n, \tag{33}$$

$$J_{3,ijk}^{DD} = \sum_{n=0}^{4} c_{n,ijk} \eta^n \tag{34}$$

with the coefficients:

$$a_{n,ij} = a_{0n} + \frac{(m_i m_j)^{1/2} - 1}{(m_i m_j)^{1/2}} a_{1n} + \frac{(m_i m_j)^{1/2} - 1}{(m_i m_j)^{1/2}} \cdot \frac{(m_i m_j)^{1/2} - 2}{(m_i m_j)^{1/2}} a_{2n}, \tag{35}$$

$$b_{n,ij} = b_{0n} + \frac{(m_i m_j)^{1/2} - 1}{(m_i m_j)^{1/2}} b_{1n} + \frac{(m_i m_j)^{1/2} - 1}{(m_i m_j)^{1/2}} \cdot \frac{(m_i m_j)^{1/2} - 2}{(m_i m_j)^{1/2}} b_{2n}, \tag{36}$$

$$c_{n,ijk} = c_{0n} + \frac{(m_i m_j m_k)^{1/3} - 1}{(m_i m_j m_k)^{1/3}} c_{1n} + \frac{(m_i m_j m_k)^{1/3} - 1}{(m_i m_j m_k)^{1/3}} \cdot \frac{(m_i m_j m_k)^{1/3} - 2}{(m_i m_j m_k)^{1/3}} c_{2n}. \tag{37}$$

The universal model constants in Eqs. 35–37 are given in the work of Gross and Vrabec [33].

The effective dipole moments μ_i^{eff} is obtained by the implicit equation:

$$\mu_i^{\mathrm{eff}} = \mu_i - kT\,\alpha_i \left(\frac{1}{x_i} \frac{\partial}{\partial \mu_i^{\mathrm{eff}}} \left(\frac{A'^{\mathrm{dipole}}}{NkT} \right) \right)_{\rho,T}, \tag{38}$$

which has to be solved iteratively using Eq. 28.

If the molecular polarizability α_i is set to zero, the second term in Eq. 38 vanishes and the permanent dipole moment is used instead of the induced dipole moment. The second term in Eq. 27 also vanishes and thus, the dipolar term of Gross and Vrabec [33] is recovered, neglecting any effects due to the polarizability of the induced dipoles.

Density

The density at a given system pressure P^{sys} must be determined iteratively by adjusting the reduced density η until $P^{\text{calc}} = P^{\text{sys}}$. The number density of molecules ρ is calculated from η through:

$$\rho = \frac{6}{\pi}\eta \cdot \left(\sum_i x_i m_i d_i^3\right)^{-1}. \tag{39}$$

Pressure

Equations for the compressibility factor will be derived using the thermodynamic relation:

$$Z = 1 + \rho \left(\frac{\partial (A^{\text{res}}/nRT)}{\partial \rho}\right)_{T,n_{\text{i}}}, \tag{40}$$

where to n_i the number of moles of component i and and $nRT = NkT$.
The pressure can be calculated in units of $\text{Pa} = \text{N}/\text{m}^2$ by applying the relation:

$$P = Z \cdot kT\rho \cdot \left(10^{10}\frac{\mathring{A}}{m}\right)^3. \tag{41}$$

Fugacity Coefficient

The fugacity coefficient $\varphi_{\text{k}}(T,P)$ is related to the residual chemical potential according to:

$$RT \ln \phi_{\text{i}} = \left(\frac{\partial A^{\text{res}}}{\partial n_{\text{i}}}\right)_{T,V,n_{k\neq i}} - RT \ln Z. \tag{42}$$